SUPPLEMENTAL MATERIAL

Estimating total cerebral microinfarct burden from diffusion-weighted imaging

Eitan Auriel, MD, MSc; M. Brandon Westover, MD, PhD; Matt T Bianchi, MD, PhD; Mahmut Edip Gurol, MD, MSc ; Yael Reijmer, PhD; Sergi Martinez-Ramirez, MD ; Jun Ni, MD; Ellis Van Etten , MD; Matthew P Frosch, MD ,PhD; Panagiotis Fotiadis; Kris Schwab; Anastasia Vashkevich; Grégoire Boulouis, MD; Alayna P Younger ; Keith A Johnson, MD; Reisa A Sperling, MD, MSc ; Trey Hedden, PhD; Anand Viswanathan, MD, PhD; Steven M Greenberg, MD, PhD

Supplementary Methods

Neuropathologic examination

Following autopsy of this 56 year old man, the left hemisphere was fixed in buffered formalin and cut in the coronal plane into 16 0.5-to-1cm thick slabs as described [1] . Two standard ("1x3" glass slide) paraffin blocks were taken from each slab, one from the lateral aspect and the other from the medial surface. The samples of the lateral aspect of the hemisphere were aligned along the anterior-posterior axis to follow the contour of the middle frontal gyrus with continuity along the lateral aspect of the hemisphere to the occipital pole. Those on the medial aspect were taken at the same level along the superior-inferior axis but along the medial surface of the hemisphere. Because the spacing of slabs was partially driven by anatomic landmarks (optic chiasm, mammillary bodies, etc), tissue sampling from the slabs should be considered as semi-unbiased.

All blocks were routinely processed and stained with LH&E or H&E. Slides were reviewed by three observers including one experienced diagnostic neuropathologist (EA,YDR, MPF), and CMI were counted on each slide. Diagnostic features for a CMI were evidence of loss of normal cells (neurons, oligodendrocytes) and reactive gliosis; more acute lesions often contained macrophages with debris. Lesions with substantial hemosiderin were not included, as these were interpreted as CMB. A histogram of the number of CMIs counted per tissue section is shown in Figure II.

Estimation Model

Our binomial model implies that the probability of any single lesion occurring within the detectability temporal window, being large enough to be detected and occurring within the slices where is $p\gamma$. The probability that at least one of the n lesions that occur each year is detected is equal to the complement of the probability that none of the n lesions are detected. This latter probability is the probability that any given lesion goes undetected, $(1-p\gamma)$, multiplied by itself n times, $(1-p\gamma)^n$ (as CMIs are independent events). Therefore, the complement is

$$f(n; p, \gamma) = 1 - (1-p\gamma)^{n}$$

We also analyzed the converse question: If we see a single DWI lesion, what is the most likely underlying rate or range of rates at which lesions may be accruing? We estimate this by maximum likelihood estimate (MLE): we calculate the probability of seeing κ DWI lesions on a single random scan as a function of the underlying annual rate *n*. In our model the probability of detecting κ lesions on an MRI when the underlying rate is *n* (with $p\gamma$ as the probability of detecting any one of these independent events) is:

$$h(\kappa|n, \rho, \gamma) = (\kappa\ ) (\rho\gamma)^{\kappa} (1-\rho\gamma)^{n-\kappa}$$

To assess the additional effect of negative DWI scans on the MLE, and 95% confidence intervals, we generated 10^6 runs of Monte Carlo simulation over a very wide range of underlying CMI rate *r* (between 0 and 3650 lesions per year). For each run, new lesion occurrence over 10 day periods was simulated following a Poisson process (equal probability of occurrence at any given instant, and average rate equal to *r*). The MLE (or 95% CI) for having the observed combination of 1 DWI-positive and 2 DWI-negative scans (Table I) were calculated from the underlying lesion rate that most often produced this combination of scan results (or that contained 95% of the trials producing this combination of results) over the 10^6 simulated runs.

Table I. Effect of negative DWI scans on annual lesion rate.

DWI-positive MRI scans/ Total MRI scans	Underlying annual rate of CMI (95% CI)*
0/3	0-1050
1/3	1051-2529
2/3	2530-5058
3/3	>5059

*** Estimates performed at γ=1%**

Supplemental Figure Legends

Figure I Size distribution of CMI diameters. The plot shows the kernel estimate of the distribution of CMI diameters generated from measurements performed in the Religious Orders Study [2,3] The actual measured diameters are shown as red '+' signs below the estimated distribution

Figure II Numbers of CMI per pathological slide from the brain of the 56 year old man with an incidental DWI lesion during life

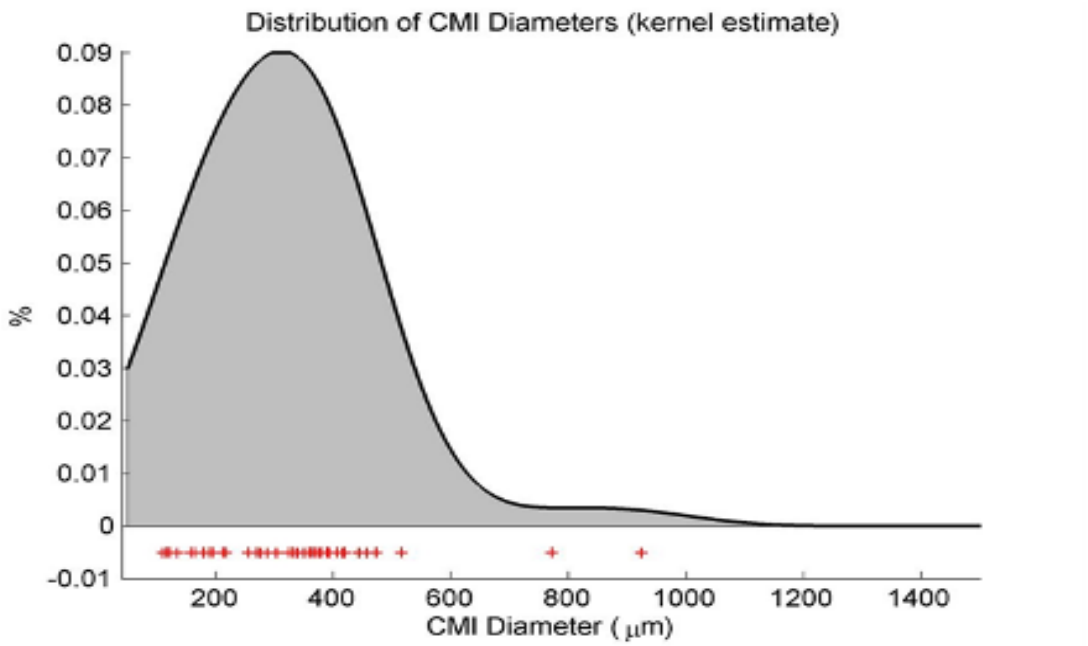
Distribution of CMI Diameters (kernel estimate)
0.09
0.08
0.07
0.06
0.05
0.04
0.03
0.02
0.01
0
-0.01
%
200
400
600
800
1000
1200
1400
CMI Diameter (μm)

Figure I

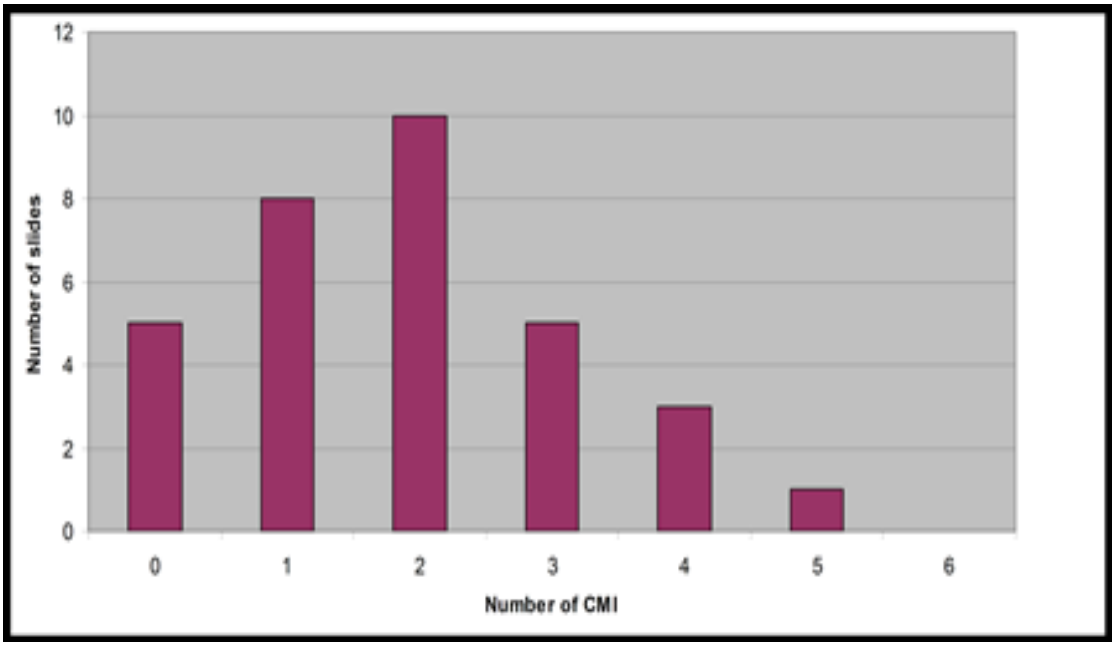

Figure II

Supplemental References

1.Vonsattel JP, Aizawa H, Ge P, DiFiglia M, McKee AC, MacDonald M, et al. An improved approach to prepare human brains for research. J. Neuropathol. Exp. Neurol. 1995; 54: 42–56.

2.Westover MB, Bianchi MT, Yang C, Schneider JA, Greenberg SM. Estimating cerebral microinfarct burden from autopsy samples. Neurology 2013; 80: 1365–1369.

3.Arvanitakis Z, Leurgans SE, Wang Z, Wilson RS, Bennett DA, Schneider JA. Cerebral amyloid angiopathy pathology and cognitive domains in older persons. Ann. .Neurol. 2011; 69: 320–327

.